

CHEMISTRY

Electronic landscape of the *f*-electron intermetallics with the ThCr₂Si₂ structure

You Lai^{1,2}, Julia Y. Chan³, Ryan E. Baumbach^{1,2*}

Although strongly correlated *f*-electron systems are well known as reservoirs for quantum phenomena, a persistent challenge is to design specific states. What is often missing are simple ways to determine whether a given compound can be expected to exhibit certain behaviors and what tuning vector(s) would be useful to select the ground state. In this review, we address this question by aggregating information about Ce, Eu, Yb, and U compounds with the ThCr₂Si₂ structure. We construct electronic/magnetic state maps that are parameterized in terms of unit cell volumes and *d*-shell filling, which reveals useful trends including that (i) the magnetic and nonmagnetic examples are well separated, and (ii) the crossover regions harbor with exotic states. These insights are used to propose structural/chemical regions of interest in these and related materials, with the goal of accelerating discovery of the next generation of *f*-electron quantum materials.

INTRODUCTION

Interest in strongly correlated *f*-electron intermetallics is periodically renewed by discoveries of exemplary materials with remarkable behaviors [e.g., hidden order and superconductivity in URu₂Si₂ (1), anomalously high temperature superconductivity in PuCoGa₅ (2), topological insulating behavior in SmB₆ (3), strongly correlated Weyl-Kondo semimetallic behavior in Ce-based compounds (4), and heavy fermion superconductivity in many Ce- and U-based systems (5, 6)]. The vitality of this cycle was recently seen in the emergence of unconventional spin triplet superconductivity in UTe₂ (7, 8), which features anomalously large upper critical fields and magnetic field-driven reentrant superconductivity. Even among the heavily studied variants of the ThCr₂Si₂ structure, this trend toward serendipitous discovery is alive and well. For example, CeRh₂As₂ (CaBe₂Ge₂-type structure) was recently shown to exhibit unconventional superconductivity, anomalously large upper critical fields, and evidence for several superconducting order parameters (9, 10). Both of these materials may even feature nontrivial electronic topologies.

These types of discoveries clearly invite continued efforts to develop *f*-electron intermetallics, but the field is hampered by a lack of clarity regarding where to look for examples with enhanced properties. This is largely because (i) the relative strengths of interactions (e.g., Kondo, RKKY, valence instability, spin orbit, crystal electric field splitting, etc.) vary widely between different materials, (ii) unusual states often emerge as a result of finely balanced or cumulative interactions, and (iii) calculations to quantify the relative importance of different interactions often have limited success. Historically, this has necessitated systematic experimental surveys of the chemical/structural phase space to uncover materials with novel electronic and magnetic states (11). However, it is also widely held that these resource-intensive surveys are not optimal—at least in the sense that the discovery of examples with remarkable physics requires sifting through a large number of related examples.

What is often missing in this process is a simple way to determine whether a given compound can reasonably be expected to exhibit

novel behavior (either intrinsically or under modest tuning) and what tuning vector(s) would be useful. Here, we address this challenge by reexamining the families of materials with the AT₂X₂ composition (12, 13), where we show that for the A = Ce-, Eu-, Yb-, and U-based subsets with the ThCr₂Si₂-type structure, (i) the magnetic and nonmagnetic examples are well separated, (ii) the crossover region that separates them follows a simple but nontrivial trajectory, and (iii) the crossover region hosts the examples that exhibit attractive behavior such as unconventional superconductivity and non-Fermi liquid behavior. These observations are consistent with earlier organizing principles [e.g., the Doniach phase diagram (14), the Hill plot (15), and surveys of Ce- and U-based 122 compounds (16–18) that emphasize electronic hybridization strength] but have the benefit that they (i) clarify chemical strategies to search for new examples with novel behavior and (ii) provide a concise summary of behaviors in this structural family. We also suggest that this approach is well suited to elementary data mining of electronic databases that can be used to investigate many other structural families.

STRUCTURE, CHEMISTRY, AND GENERIC PHASE DIAGRAMS

The ThCr₂Si₂ structure (Fig. 1A) was first reported by Ban and Sikirica in (12), and since then, it has proven to be one of the most ubiquitous structural arrangements for ternary combinations of elements. There are many detailed reviews that address trends in this family, and several are listed in (13). To summarize, it is a ternary variant of the BaAl₄ prototype (space group *I4/mmm*) and is generically expressed as AT₂X₂, where the A, T, and X atoms are located on the Wyckoff sites 2a (0,0,0), 4d (0,0.5,0.25), and 4e (0,0,z), respectively. This provides distinct high-symmetry environments around the A, T, and X atoms that influence the physical properties of the chemical variants. This structure also exhibits pronounced chemical flexibility, where the A site can be populated by alkali metal, alkaline earth, rare earths, first column transition metals, lanthanide, and actinide elements; the T site can be occupied by transition metal, light alkali metals and alkaline earths, and *p*-block elements; and the X site can be occupied by *p*-block elements and some transition metals. There are many other closely related structures [e.g., CaBe₂Ge₂, CeNiSi₂, BaNiSn₃, and U₂Co₃Si₅ types (19–22)], and there are even hybrid examples that combine this family and other prototypes

¹National High Magnetic Field Laboratory, Florida State University, Tallahassee, FL 32310, USA. ²Department of Physics, Florida State University, Tallahassee, FL 32306, USA. ³Baylor University, Waco, TX 76706, USA.

*Corresponding author. Email: baumbach@magnet.fsu.edu

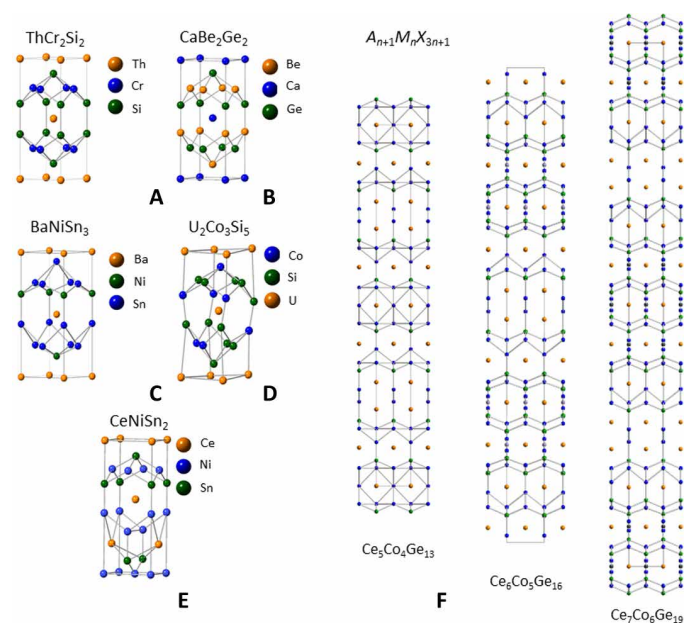


Fig. 1. Summary of crystalline structures that relate to the ThCr_2Si_2 prototype. (A to E) The ThCr_2Si_2 , CaBe_2Ge_2 , BaNiSn_3 , $\text{U}_2\text{Co}_3\text{Si}_5$, and CeNiSi_2 structures taken from (12, 13, 19–22). (F) The structure for the $A_{n+1}M_nX_{3n+1}$ (A = lanthanide, M = transition metal, X = tetrels), $n = 4$ to 6 compounds, composed of complex layering of subunits. Ce, Co, and Ge are represented as orange, green, and blue spheres, respectively. Structural details obtained from (23–25).

(Fig. 1, B to F) (23–25), which opens the prospect of developing design principles that span families of materials.

A multitude of behaviors emerge from these simple crystal structures when f -elements are introduced into them, including local moment and complex magnetism (26), charge instabilities (27), structural instabilities (28), unconventional superconductivity (29, 30), hidden order (1), multipolar order (31), and topologically protected electronic states (9, 10). For the Ce-, Yb-, and U-based systems, the behavior is especially rich and is often understood in terms of the Ruderman-Kittel-Kasuya-Yosida (RKKY) and Kondo interactions (14, 32–35), where (i) the RKKY interaction provides an indirect magnetic exchange between localized f -spins through the conduction electrons and favors magnetic ordering while (ii) the Kondo interaction drives hybridization between the conduction electron and f -states that results in screening of the f -spin and strongly reduces the effective magnetic moment. The connection between these parameters has been discussed extensively in terms of the Doniach model and is summarized in (5, 6). The resulting generic phase diagrams are shown schematically in Fig. 2 (A and B) for Ce and Yb, where a tuning parameter δ (e.g., pressure or chemical substitution) varies the ground state. For the case of Ce, at small δ , the valence is close to 3+, hybridization between the f - and conduction electrons is weak, and there typically is a magnetically ordered ground state at $T_{N,C}$. As δ increases, $T_{N,C}$ may initially increase as the RKKY interaction strengthens, but eventually, it tends to be suppressed toward zero temperature at δ_c . Under some conditions, this results in a quantum critical point that is surrounded by a fan-like region of non-Fermi liquid behavior. For many CeT_2X_2 compounds, the quantum critical point is also surrounded by a dome of unconventional superconductivity. At larger δ , the hybridization strength increases

further, Fermi liquid behavior is observed below a crossover temperature T_{FL} , and eventually intermediate valence or a tetravalent state emerges. The Ce and Yb phase diagrams are related but are inverted with respect to each other owing to how Hund's rules determine the total angular momentum J : for Ce^{3+} ($J = 5/2$) and Ce^{4+} ($J = 0$), and for Yb^{2+} ($J = 0$) and Yb^{3+} ($J = 7/2$).

Some lanthanide- and actinide-based materials with multiple f -orbitals exhibit related phase diagrams, but additional complexities are involved. For example, a semi-universal phase diagram has been proposed for Eu-based intermetallics (36, 37), which resembles the Doniach picture but also includes distinct features relating to the valence transition between the Eu^{2+} ($J = 7/2$) and Eu^{3+} ($J = 0$) states (Fig. 2C). There is also an ongoing debate about the importance of valence instabilities in Ce- and Yb-based materials, their role in determining classes of quantum criticality, and impact on superconductivity (38–40). We point out that related behavior might even be expected in families containing Pr, Sm, and Tm where multiple valence states are available (41, 42). Among actinide-based materials, the situation is even more complicated due to the greater tendency toward f -state itinerancy, the potential impact of relativistic effects, and the presence of multiple f -electron orbitals that could experience differing degrees of hybridization (43). Nonetheless, phase diagrams that resemble those shown in Fig. 2 (A to C) are sometimes observed (44, 45). Last, all of these behaviors should be contrasted with those of the remaining lanthanides, where (i) the valence is rigidly fixed to be trivalent and (ii) hybridization between the conduction electron and f -states is weak.

On the basis of these observations, it is appealing to suggest that although there are wide-ranging behaviors in this family of materials, the QCP scenario provides a powerful design principle for producing examples with attractive behaviors. However, even with these insights, it remains unclear (i) which ones are best suited to further investigations because they are near a magnetic or valence instability and (ii) for a given material (or family of materials) what is the best tuning strategy to access regions of interest. To address this, we assemble maps in the chemical-structural phase space for the compounds $(\text{Ce}, \text{Yb}, \text{Eu}, \text{U})\text{T}_2\text{X}_2$ with the ThCr_2Si_2 structure and identify regions of interest. We also comment on related structures and prospects for uncovering novel phenomena in them.

ELECTRONIC-MAGNETIC MAPS FOR $(\text{Ce}, \text{Yb}, \text{Eu}, \text{U})\text{T}_2\text{X}_2$ WITH THE ThCr_2Si_2 STRUCTURE

Figure 3A presents the phase map for the compounds CeT_2X_2 (T = transition metal and X = Si, Ge) by providing the lattice constants and f -state as reported in literature (16–18, 29, 40, 46–77). By organizing these compounds based on their transition metal column and unit cell volume, it is seen that (i) there is a clear separation between those with trivalent Ce and tetravalent or intermediate valence Ce; (ii) the crossover region includes all of the examples that exhibit Kondo lattice heavy fermion, quantum criticality, non-Fermi liquid, and superconducting behavior; and (iii) the crossover region depends on a nearly linear relationship between shell filling and unit cell volume. Points (i) and (ii) are illustrated by the evolution from a strongly hybridized Kondo lattice (CeCu_2Si_2) toward weakened hybridization and strengthened magnetism as the unit cell volume increases (29). This is also noticeable for the other isovalent transition metal series, which all go from tetravalent examples [e.g., CeNi_2Si_2 (61)] through strongly hybridized Kondo lattices

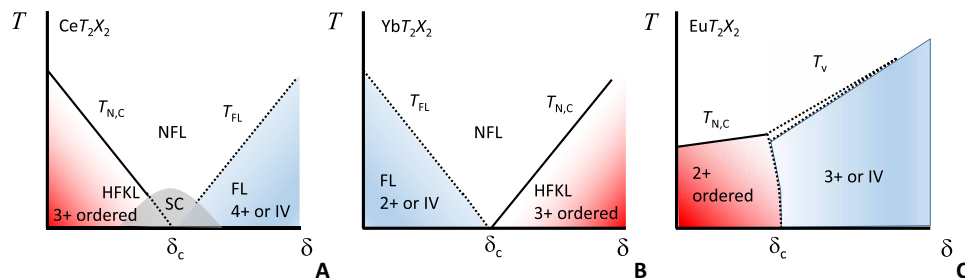


Fig. 2. Schematic phase diagrams for strongly correlated *f*-electron intermetallics. Temperature T versus control parameter δ phase diagram for the compounds (A) CeT_2X_2 (5, 6), (B) YbT_2X_2 (5, 6), and (C) EuT_2X_2 (36, 37), where T = transition metal and X = p -block element. Here, δ is the chemical composition x or pressure P . The trends for the magnetic ordering temperatures $T_{N,C}$, superconducting transition temperatures T_C , valence change transition temperatures T_V , and Fermi liquid crossovers T_{FL} that are observed in these phase diagrams are described in the text. The solid lines represent phase boundaries, whereas the dotted lines represent crossover regions: e.g., temperature ranges over which a system enters a Fermi liquid or intermediate valence (IV) ground state. The *f*-electron valences are also indicated (3+ or 4+ for cerium, 2+ or 3+ for ytterbium, and 2+ or 3+ for europium). Note that these diagrams focus on the critical regions near δ_c , but the more general Doniach phase diagram includes a region where the ordering temperatures increase with δ as the RKKY interaction strengthens, before collapsing toward $T=0$ at δ_c (14). This trend is seen in the ordering temperatures presented in Fig. 3.

[e.g., CeNi_2Ge_2 (60, 61)] to trivalent cerium magnetism [CePd_2Ge_2 (59, 60)]. Supporting evidence for this evolution is seen by examining the unit cell volume lanthanide contractions for each family of materials, where reductions from the trivalent lanthanide contraction are seen for tetravalent or intermediate valence examples. Related behavior is observed for many other cerium-based intermetallics and is generally understood in the context of the Doniach picture or in terms of empirical frameworks such as Hill plots (Fig. 2A) (6, 14, 15).

The effect of non-isoelectronic tuning is less easily anticipated but is clarified by earlier studies showing that the hybridization strength between the *f*-electron and conduction electron states tends to decrease going from the iron column toward the copper column (16–18). Within the Ce-map, the importance of this is seen for the group of materials with unit cell volumes near 170 \AA^3 , where there is a progression from intermediate valence or tetravalent behavior [CeOs_2Si_2 (51)] to heavy fermion Kondo lattice behavior [CeIr_2Si_2 (56)], to quantum-critical non-Fermi liquid behavior and superconductivity [CeNi_2Ge_2 (60, 61)], and lastly trivalent magnetic ordering [$\text{CeCu}_2(\text{Si}_{1-x}\text{Ge}_x)_2$ at $x \approx 0.2$ (66)]. This illustrates that weakening hybridization causes the boundary between magnetic (Ce^{3+}) and nonmagnetic (Ce^{4+} or intermediate valence) behavior to shift toward smaller unit cell volumes with increasing *d*-shell filling. Outside of this crossover region, horizontal lines always traverse either intermediate valence or tetravalent cerium states (small volumes) or trivalent cerium states with magnetic ordering (large volumes).

The examples that exhibit heavy Fermi liquid Kondo lattice behavior, superconductivity, or non-Fermi liquid behavior [e.g., CeRu_2Si_2 (50), CeCu_2Si_2 (29), and CeNi_2Ge_2 (60, 61)] appear at the boundary between the two regions and are readily tuned through it by changing either the unit cell volume or the *d*-shell filling. For example, in the cases of CeCu_2Si_2 and CeNi_2Ge_2 , applied pressure drives the ambient pressure superconducting transition through a dome-like region (29, 60). Fermi liquid behavior that is consistent with the system entering either an intermediate valence or tetravalent cerium state emerges at large pressures, where a second dome of superconductivity is observed. In contrast, isoelectronic chemical substitution that expands the lattice drives these compounds into magnetic ground states where the hybridization strength is reduced. It is also seen that the examples with magnetically ordered

ground states that are near the boundary [e.g., CePd_2Si_2 (60) and CeRh_2Si_2 (54)] are readily moved into it using applied pressure, while larger pressures are needed to move more distant examples [e.g., CeAu_2Si_2 (40) and CeCu_2Ge_2 (67)] into the crossover region. Non-isoelectronic chemical substitution series reveal related trends: e.g., when antiferromagnetic $\text{Ce}(\text{Cu}_{1-x}\text{T}_x)_2\text{Ge}_2$ ($x = 0$) is chemically substituted by $T = \text{Ni}$ or Co , the boundary region is crossed and critical behavior is observed over a limited x -range (47, 69).

Thus, it is clear that for the entire $\text{CeT}_2(\text{Si,Ge})_2$ series, the region that separates the magnetic and nonmagnetic members varies systematically with both the unit cell volume and the electronic shell filling, each tuning the hybridization strength in a distinct way. This perspective is reinforced by considering the related maps for the compounds CeT_2X_2 (T = transition metal and $X = \text{P, As}$; Fig. 3B) (70–77). Although it is less clear in this case, we infer from these data and the trends that are seen for the Si/Ge analogs that there is a similar non-trivial vector separating the magnetic and nonmagnetic regions. As before, the examples that exhibit strongly correlated electron physics [e.g., CeRu_2P_2 (71)] are on the boundary.

Given the success of this simple scheme in describing the Ce-based ThCr_2Si_2 compounds, we next examine the maps for the Yb examples (Fig. 4) (30, 31, 78–97). Note that few pnictide analogs have been reported, so a map is not included. For the Si/Ge series, there is a strong resemblance between the Yb and Ce maps, but the magnetic and nonmagnetic regions are inverted. This is due to Hund's rules producing $J = 7/2$ for trivalent ytterbium ($4f^{13}$), while divalent Yb has a full *f*-shell ($4f^{14}$ and $J = 0$). In the intermediate volume region, there are several nearly critical Kondo lattice systems, as well as the well-known quantum critical material YbRh_2Si_2 (30, 84). Chemical substitution studies have been performed for many of these examples: e.g., (i) $\text{Rh} \rightarrow \text{Co}$ substitution in YbRh_2Si_2 stabilizes magnetism, weakens the hybridization strength, and leads to magnetic ordering (97); (ii) applied pressure drives YbFe_2Ge_2 from being a heavy fermion Kondo lattice through a quantum critical point with non-Fermi liquid behavior, into an antiferromagnetically ordered ground state (80); and (iii) applied pressure drives divalent YbCu_2Ge_2 toward intermediate valence behavior (94). Similar behavior is seen for tuning studies of other examples such as YbIr_2Si_2 (83), YbCu_2Si_2 (95), and YbPd_2Si_2 (96). These observations suggest that the hybridization strength for the Yb compounds is strongly

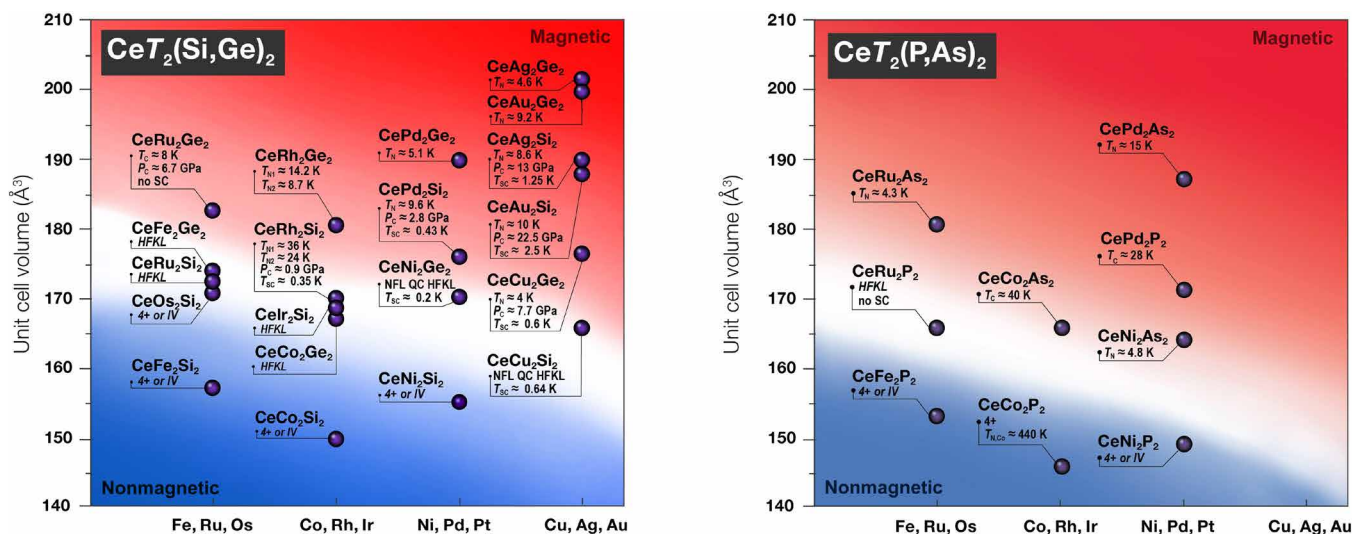


Fig. 3. Phase map for the valence and ground state behavior of the compounds CeT_2X_2 ($T = \text{transition metal and } X = \text{Si/Ge and P/As}$) that crystallize in the $ThCr_2Si_2$ -type structure (16–18, 29, 40, 46–77). The axes that control the ground state are the unit cell volume (V) and the d -shell filling going from the Cu column to the Fe column. The white band that traverses the center of the phase diagram is a guide to the eye that approximately separates the examples with trivalent cerium [lower left-hand side (blue background)] from those with trivalent cerium [upper right-hand side (red background)]. Ordering temperatures are labeled (Neel temperature T_N and Curie temperature T_C). Also shown in some cases are the critical pressures where magnetism collapses (P_C) and the associated superconducting transition temperature (T_C). These values and their associated references are summarized in table S1.

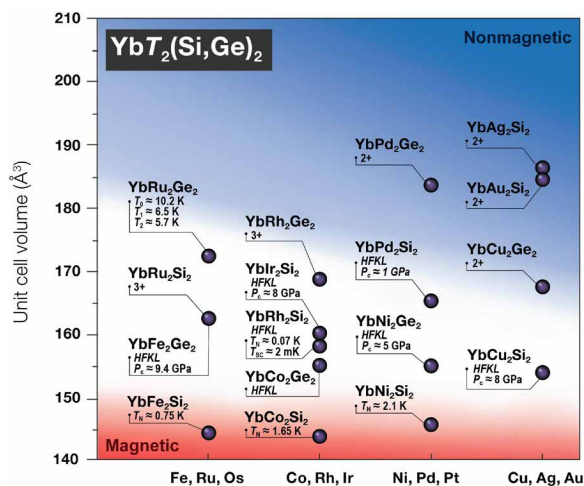


Fig. 4. Phase map for the valence and ground state behavior of the compounds YbT_2X_2 ($T = \text{transition metal and } X = \text{Si/Ge}$) that crystallize in the $ThCr_2Si_2$ -type structure (30, 31, 78–97). The white band that traverses the center of the phase diagram is a guide to the eye that approximately separates the examples with trivalent [bottom (red background)] from those with divalent ytterbium [upper right-hand side (blue background)]. Ordering temperatures are labeled (Neel temperature T_N and Curie temperature T_C). Critical pressures P_C are labeled. These values and their associated references are summarized in table S2.

controlled by a combination of lattice contraction and d -shell filling in a manner that resembles what is seen for the Ce analogs.

It is also of interest to examine other Pr-, Sm-, Eu-, and Tm-based compounds that potentially could exhibit valence instabilities (41, 42). Among this group, those with Pr, Sm, and Tm so far show no evidence in their bulk properties for crossover regions. This is supported by inspection of the evolution of their unit cell volumes,

where all examples conform to the trivalent lanthanide contraction. This leads us to expect that although these families might, in principle, include interface regions, they are not within the chemical phase space of the naturally occurring examples in this structure.

In contrast, the Eu compounds show trends that are related to the Ce and Yb analogs (Fig. 5) (36, 37, 98–131). The compressed volume examples all exhibit either trivalent ($4f^6$, $J = 0$) or intermediate valence behavior while the expanded volume examples exhibit divalent ($4f^7$, $J = 7/2$) behavior. Examples close to the crossover region are readily tuned through it: e.g., the Eu valence and unit cell volume of $EuCu_2Si_2$ vary between 2+ and 3+ depending on synthesis method (115, 116) while $EuIr_2Si_2$ exhibits behavior that is similar to what is seen in Kondo lattice systems with modest hybridization strength (104). When the antiferromagnets $EuNi_2Ge_2$ (108) and $EuRh_2Si_2$ (102) are compressed using hydrostatic pressure, they evolve toward Kondo lattice-like behavior similar to that of $EuIr_2Si_2$. Remarkable behavior is seen for $EuPd_2Si_2$, which is nearly divalent at room temperature but its temperature-dependent volume contraction is sufficient to drive a phase transition into the trivalent state (36, 107). Among the pnictides, it is noteworthy that although most of them exhibit a divalent state, the heavy fermion Kondo lattice $EuNi_2P_2$ appears to be in a crossover region where the critical unit cell volume is substantially smaller than that of the Si/Ge analogs (130, 131). These maps also reveal an important distinction from the Ce and Yb analogs, since here the electronic shell filling has a negligible impact on the location of the crossover region.

Last, Fig. 6 summarizes results for the compounds UT_2X_2 (1, 79, 132–146). There are a limited number of pnictide examples, so we focus on the Si/Ge group. Again, there is a separation between the magnetic and nonmagnetic examples, but in this case, the latter group is clustered around the Fe/Ru/Os transition metal group. Most of these compounds are Pauli paramagnets [e.g., UFe_2Si_2 (134), UFe_2Ge_2 (133), and UOs_2Si_2 (132)] where strong hybridization between the

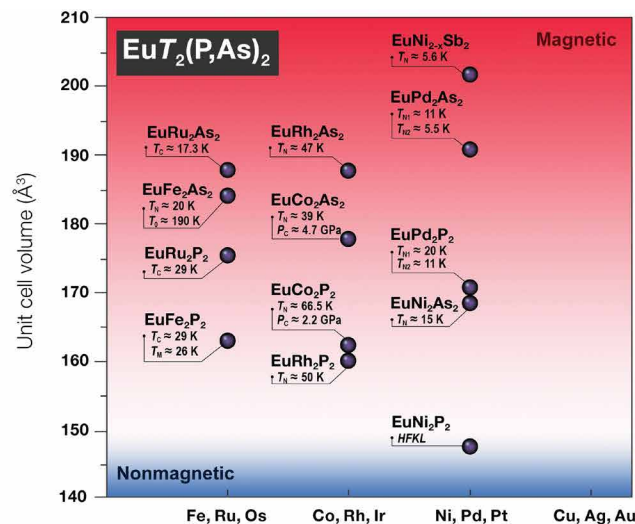
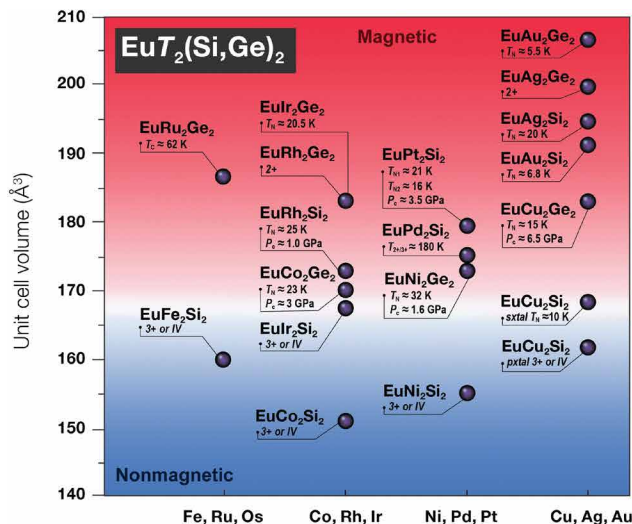


Fig. 5. Phase map for the valence and ground state behavior of the compounds EuT_2X_2 (T = transition metal and X = Si/Ge and P/As) that crystallize in the ThCr_2Si_2 -type structure (36, 37, 98–131). The white band that traverses the center of the phase diagram is a guide to the eye that separates the examples with trivalent or intermediate valence europium [lower half (blue background)] from those with divalent europium [upper half (red background)]. Ordering temperatures are labeled (Neel temperature T_N and Curie temperature T_C). Critical pressures P_C are labeled. These values and their associated references are summarized in table S3.

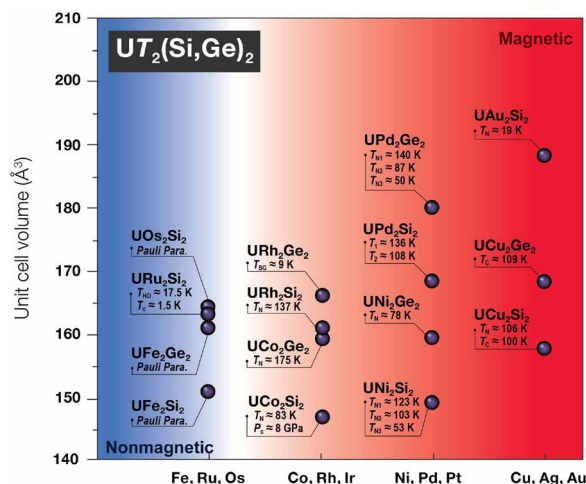


Fig. 6. Phase map for the valence and ground state behavior of the compounds UT_2X_2 (T = transition metal and X = Si/Ge) that crystallize in the ThCr_2Si_2 -type structure (1, 79, 132–146). The white band separates the examples with Pauli paramagnetism [left-hand side (blue background)] from those with magnetically ordered ground states [right-hand side (red background)] is a guide to the eye. Ordering temperatures are labeled (Neel temperature T_N , Curie temperature T_C , hidden order temperature T_{HO} , spin glass temperature T_{SG} , and superconducting transition temperature T_C). Critical pressures P_C are labeled. These values and their associated references are summarized in table S4.

f - and conduction electron states causes the f -state to become delocalized. It is interesting to note that the hidden order compound, URu_2Si_2 , is located in close vicinity to these examples, which is consistent with the view that strong hybridization plays an important role in this material (1). Similar to what is seen for the lanthanides, the hybridization strength weakens going toward the Cu/Ag/Au column (16, 17). The result is that the remainder of the compounds all exhibit magnetic ground states with large ordering temperatures.

Some of these examples host complex magnetism [e.g., spin glass behavior in URh_2Ge_2 (135) and multiple phase transitions in many others] and are susceptible to disorder effects, but these behaviors do not appear to be associated with the crossover region. Decreases in the unit cell volume tend to slowly suppress the ordering temperature, but in contrast to the Ce, Yb, and Eu analogs, there is no volume-driven crossover region for this family. Instead, large pressures are needed to access it, as demonstrated for UCo_2Si_2 that has a critical pressure near 8 GPa (140). For UNi_2Si_2 and UCu_2Si_2 , even larger pressures would be needed, as experiments have so far been unsuccessful in fully suppressing the magnetism (141, 146). Thus, it is clear that the U series is distinct from the Ce, Yb, and Eu analogs in terms of the conditions that would be useful for driving critical behavior. This has been remarked upon previously (146) and likely reflects differences between the $5f$ and $4f$ states. Such information is of high importance in developing tuning strategies to access the critical region.

OUTLOOK FOR FUTURE EFFORTS

These insights are immediately useful for focusing investigations of materials with the ThCr_2Si_2 structure. For example, although the Ce-series has already been extensively studied, there remain some attractive examples that have not received close attention. CeCo_2As_2 (73) is of interest because it is simultaneously near the crossover region and may also exhibit strong d -electron magnetism similar to what is seen for CeCo_2P_2 (74). Preliminary results reveal ferromagnetic ordering at $T_C \approx 40$ K (73), and we speculate that the ordered state would be readily suppressed using applied pressure, $\text{As} \rightarrow \text{P}$ substitution, or $\text{Co} \rightarrow \text{Fe}$ or Ni substitution. Examination of the Eu and Yb families reveals other opportunities. Both EuFe_2Ge_2 and EuRu_2Si_2 have not been reported, although the related compounds RFe_2Ge_2 (R = Y, Pr, Nd, Sm, Gd-Tm, and Lu) and EuT_2Ge_2 (T = transition metal) are described in (147, 148). Here, it was inferred that EuFe_2Ge_2 is not a stable phase under conventional growth conditions. This

leads us to propose that this phase, and others that are “missing” from the maps, might be accessible as metastable phases where modest amounts of applied or chemical pressure might be sufficient to stabilize them. If they can be formed, they might exhibit complex phase diagrams involving valence instability physics similar to what is seen in EuPd_2Si_2 (36, 107), EuRh_2Si_2 (102), or EuCo_2Ge_2 (103), where modest lattice contractions are sufficient to access the valence change region. The heavy fermion Kondo lattice EuNi_2P_2 appears to be within the crossover region and exhibits Kondo lattice–like behavior (130, 131). This invites efforts to traverse the crossover region using chemical substitution. Last, for the Yb-based examples, we note that there have already been substantial efforts, where the focus has been on the prototypical quantum critical point material YbRh_2Si_2 (30, 84). Nonetheless, there are several other remarkable materials in this family including YbRu_2Ge_2 (31), which exhibits quadrupolar order and strongly correlated electron behavior. This is unique among all other lanthanide-based materials with the ThCr_2Si_2 structure and motivates chemical substitution studies that span the crossover region.

The U-based examples show distinct trends that draw attention toward d -shell filling as being the only viable route for entering the crossover region. This perspective has already been explored for URu_2Si_2 (149, 150), where electronic shell filling produces a semi-universal T - x phase diagram with three main regions: (i) The hidden order state is rapidly suppressed toward zero temperature for $x \lesssim x_{\text{cr},1}$, (ii) paramagnetism with a heavy-Fermi liquid ground state is seen for $x_{\text{cr},1} \lesssim x \lesssim x_{\text{cr},2}$, and (iii) complex antiferromagnetic order appears for $x_{\text{cr},2} \lesssim x$. Unexpectedly, this behavior is induced regardless of the type of chemical substitution (e.g., $\text{Ru} \rightarrow \text{Rh}$, Ir , and $\text{Si} \rightarrow \text{P}$), as long as it effectively adds electrons. This motivates further studies of the nearby Pauli paramagnetic analogs, where non-isoelectronic chemical substitution can be used to tune toward the magnetic region [e.g., $\text{U}(\text{Fe}_{1-x}\text{T}_x)_2\text{Ge}_2$, where $T = \text{Co}$, Rh , and Ir].

Last, it will be valuable to use these insights to cast a wider net into the structural variants with the CaBe_2Ge_2 , CeNiSi_2 , BaNiSn_3 , and $\text{U}_2\text{Co}_3\text{Si}_5$ structure types, where a preliminary survey indicates that they exhibit maps that are similar to those presented here. Recent work has also shown that there are complex hybrid structures that combine standard building blocks with other structural elements. An example of this is seen for the homologous series $A_{n+1}M_nX_{3n+1}$ ($A = \text{lanthanide}$, $M = \text{transition metal}$, $X = \text{tetrels}$, and $n = 1$ to 6), which are constructed from basic structural subunits such as AlB_2 , AuCu_3 , and BaNiSn_3 (Fig. 1F). Examples spanning $n = 1$ to 6 for the $A = \text{Ce}$ series have already been uncovered (23–25), where complex magnetism and Kondo lattice physics is observed. For example, $\text{Ce}_7\text{Co}_{6+x}\text{Ge}_{19-y}\text{Sn}_y$ ($n = 6$), with four crystallographically unique lanthanide sites, was recently shown to have five magnetic transitions of 5, 6, 7.2, 12.4, and 16.5 K. It was also shown that three of the $n = 6$ magnetic transitions are also found in the $n = 5$ member (24). This opens the possibility that magnetic/electronic behaviors can be controlled using varied stacking arrangements. The diversity of this behavior invites further investigations, where we expect (i) additional n variation and (ii) chemical flexibility on all of the crystallographic sites. It is easy to look forward to (i) the Eu, Yb, and U analogs being hosts for many different novel electronic/magnetic behaviors and (ii) the transition metal and tetrel sites accommodating isoelectronic replacement and possibly even nonisoelectronic substitution. While a brute force examination of the chemical phase space is not feasible, our maps offer a route forward. For example, all of the Ce-based

examples that have been uncovered so far exhibit local f -moment magnetism. Taking inspiration from the maps for the ThCr_2Si_2 Ce-based materials, this implies that efforts should be made to increase the hybridization strength by compressing the unit cell volume (e.g., using applied pressure or $\text{Ge} \rightarrow \text{Si}$ substitution) and undertaking chemical substitution studies that point toward the iron column.

SUMMARY AND CONCLUSION

In this review, we have constructed structural/chemical maps for intermetallics with the ThCr_2Si_2 structure, which reveal distinct regions where classes of f -state behaviors emerge. In particular, among the Ce, Eu, Yb, and U families, the cases with magnetic f -states are separated from those with strongly hybridized nonmagnetic f -states by a well-contained crossover region that depends on both unit cell volume and electron shell filling. The examples that exhibit emergent behavior that is associated with quantum criticality are found in the crossover region. This agrees with earlier perspectives (e.g., Doniach and Hill) but clarifies the role of chemical composition without resorting to computational methods. These insights will be useful to pinpoint regions of interest in families of materials related to the ThCr_2Si_2 prototype and have the potential to accelerate discoveries of intriguing phenomena. This approach may even be applicable to other structural families, where mining of electronic databases could be used to accelerate progress.

SUPPLEMENTARY MATERIALS

Supplementary material for this article is available at <https://science.org/doi/10.1126/sciadv.abp8264>

REFERENCES AND NOTES

- J. A. Mydosh, P. M. Oppeneer, P. S. Riseborough, Hidden order and beyond: An experimental-theoretical overview of the multifaceted behavior of URu_2Si_2 . *J. Phys. Condens. Matter* **32**, 143002 (2020).
- J. L. Sarrao, L. A. Morales, J. D. Thompson, B. L. Scott, G. R. Stewart, F. Wastin, J. Rebizant, P. Boulet, E. Colineau, G. H. Lander, Plutonium based superconductivity with a transition temperature above 18 K. *Nature* **420**, 297–299 (2002).
- M. Dzero, K. Sun, V. Galitski, P. Coleman, Topological Kondo insulators. *Phys. Rev. Lett.* **104**, 106408 (2010).
- H.-H. Lai, S. E. Grefe, S. Paschen, Q. Si, Weyl–Kondo semimetal in heavy-fermion systems. *Proc. Natl. Acad. Sci. U.S.A.* **115**, 93–97 (2018).
- C. Pfleiderer, Superconducting phases f -electron compounds. *Rev. Mod. Phys.* **81**, 1551–1624 (2009).
- M. B. Maple, R. E. Baumbach, N. P. Butch, J. J. Hamlin, M. Janoschek, Non-fermi liquid regimes and superconductivity in the low temperature phase diagrams of strongly correlated d - and f -electron materials. *J. Low Temp. Phys.* **161**, 4–54 (2010).
- S. Ran, C. Eckberg, Q.-P. Ding, Y. Furukawa, T. Metz, S. R. Saha, I.-L. Liu, M. Zic, H. Kim, J. Paglione, N. P. Butch, Nearly ferromagnetic spin-triplet superconductivity. *Science* **365**, 684–687 (2019).
- S. Ran, I.-L. Liu, Y. S. Eo, D. J. Campbell, P. M. Neves, W. T. Fuhrman, S. R. Saha, C. Eckberg, H. Kim, D. Graf, F. Balakirev, J. Singleton, J. Paglione, N. P. Butch, Extreme magnetic field-boosted superconductivity. *Nat. Phys.* **15**, 1250–1254 (2019).
- S. Khim, J. F. Landaeta, J. Banda, N. Bannor, M. Brando, P. M. R. Brydon, D. Hafner, R. Küchler, R. Cardoso-Gil, U. Stockert, A. P. Mackenzie, D. F. Agterberg, C. Geibel, E. Hassinger, Field-induced transition within the superconducting state of CeRh_2As_2 . *Science* **373**, 1012–1016 (2021).
- K. Nogaki, A. Daido, J. Ishizuka, Y. Yanase, Topological crystalline superconductivity in locally noncentrosymmetric CeRh_2As_2 . *Phys. Rev. Res.* **3**, L032071 (2021).
- P. C. Canfield, New materials physics. *Rep. Prog. Phys.* **83**, 016501 (2019).
- Z. Ban, M. Sikirica, The crystal structure of ternary silicides ThM_2Si_2 ($M = \text{Cr}$, Mn , Fe , Co , Ni , and Cu). *Acta Crystallogr.* **18**, 594–599 (1965).
- M. Shatruk, ThCr_2Si_2 structure type: The “Perovskite” of intermetallics. *J. Solid State Chem.* **272**, 198–209 (2019).
- S. Doniach, The Kondo lattice and weak antiferromagnetism. *Physica B+C* **91**, 231–234 (1977).

15. H. H. Hill, *Plutonium in 1970 and other Actinides*, W. N. Miner, Ed. (AIME, New York, 1970), p. 2.
16. T. Endstra, G. J. Nieuwenhuys, J. A. Mydosh, Hybridization model for the magnetic-ordering behavior of uranium- and cerium-based 1:2:2 intermetallic compounds. *Phys. Rev. B Condens. Matter* **48**, 9595–9605 (1993).
17. T. T. M. Palstra, A. A. Menovsky, G. J. Nieuwenhuys, J. A. Mydosh, Magnetic properties of the ternary compounds CeT_2Si_2 and UT_2Si_2 . *J. Magn. Magn. Mater.* **54–57**, 435–436 (1986).
18. R. A. Neifeld, M. Croft, T. Mihalasin, C. U. Segre, M. Madigan, M. S. Torikachvili, M. B. Maple, L. E. DeLong, Chemical environment and Ce valence: Global trends in transition-metal compounds. *Phys. Rev. B Condens. Matter* **32**, 6928–6931 (1985).
19. B. Eisenmann, N. May, W. Müller, H. Schäfer, Eine neue strukturelle variante des BaAl_4 -Typs: Der CaBe_2Ge_2 -Typ. *Z. Naturforsch. B* **27**, 1155–1157 (1972).
20. W. Dörrscheidt, H. Schäfer, Die Struktur des BaPtSn_3 , BaNiSn_3 und SrNiSn_3 und ihre Verwandtschaft zum ThCr_2Si_2 -Strukturtyp. *J. Less Common Met.* **58**, 209–216 (1978).
21. O. I. Bodak, E. I. Gladyshevskii, System cerium-nickel-silicon in the region of 0–33 at. % Ce. *Inorg. Mater.* **5**, 1754–1758 (1969).
22. L. G. Akselrud, Y. P. Yarmolyuk, E. I. Gladyshevskii, Crystal structure of the compound $\text{U}_2\text{Co}_2\text{Si}_5$. *Sov. Phys. Crystallogr.* **22**, 492–493 (1977).
23. J. B. Felder, A. Weiland, H. Hodovanets, G. T. McCandless, T. G. Estrada, T. J. Martin, A. V. Walker, J. Paglione, J. Y. Chan, Law and disorder: Special structure units—Building the intergrowth $\text{Ce}_6\text{Co}_5\text{Ge}_{16}$. *Inorg. Mater.* **58**, 6037–6043 (2019).
24. A. Weiland, K. Wei, G. T. McCandless, J. B. Felder, L. J. Eddy, R. E. Baumbach, J. Y. Chan, Strongly correlated electron behavior in a new member of the $\text{A}_{n+1}\text{B}_n\text{X}_{3n+1}$ homologous series: $\text{Ce}_7\text{Co}_6\text{Ge}_{19}$. *Phys. Rev. Mater.* **4**, 074408 (2020).
25. A. Weiland, K. Wei, G. T. McCandless, R. E. Baumbach, J. Y. Chan, Fantastic $n=4$: $\text{Ce}_5\text{Co}_{4+x}\text{Ge}_{13-y}\text{Sn}_y$ of the $\text{A}_{n+1}\text{M}_n\text{X}_{3n+1}$ homologous series. *J. Chem. Phys.* **154**, 114707 (2021).
26. N. D. Khanh, T. Nakajima, X. Yu, S. Gao, K. Shibata, M. Hirschberger, Y. Yamasaki, H. Sagayama, H. Nakao, L. Peng, K. Nakajima, R. Takagi, T. Arima, Y. Tokura, S. Seki, Nanometric square skyrmion lattice in a centrosymmetric tetragonal magnet. *Nat. Nanotechnol.* **15**, 444–449 (2020).
27. J. Lee, K. Prokes, S. Park, I. Zaliznyak, S. Dissanayake, M. Matsuda, M. Frontzek, S. Stoupin, G. L. Chappell, R. E. Baumbach, C. Park, J. A. Mydosh, G. E. Granroth, J. P. C. Ruff, Charge density wave with anomalous temperature dependence in UPt_2Si_2 . *Phys. Rev. B* **102**, 041112 (2020).
28. Y. Lai, K. Wei, G. Chappell, J. Diaz, T. Siegrist, P. J. W. Moll, D. Graf, R. E. Baumbach, Tuning the structural and antiferromagnetic phase transitions in UCr_2Si_2 : Hydrostatic pressure and chemical substitution. *Phys. Rev. Mater.* **4**, 075003 (2020).
29. H. Q. Yuan, F. M. Grosche, M. Deppe, C. Geibel, G. Sparn, F. Steglich, Observation of two distinct superconducting phases in CeCu_2Si_2 . *Science* **302**, 2104–2107 (2003).
30. E. Schubert, M. Tippmann, L. Steinke, S. Lausberg, A. Steppke, M. Brando, C. Krellner, C. Geibel, R. Yu, Q. Si, F. Steglich, Emergence of superconductivity in the canonical heavy-electron metal YbRh_2Si_2 . *Science* **351**, 485–488 (2016).
31. H. S. Jeevan, C. Geibel, Z. Hossain, Quasi-quartet crystal-electric-field ground state with possible quadrupolar ordering in the tetragonal compound YbRu_2Ge_2 . *Phys. Rev. B* **73**, 20407 (2006).
32. M. A. Ruderman, C. Kittel, Indirect exchange coupling of nuclear magnetic moments by conduction electrons. *Phys. Rev.* **96**, 99–102 (1954).
33. T. Kasuya, A theory of metallic ferro- and antiferromagnetism on Zener's model. *Prog. Theor. Exp. Phys.* **16**, 45–57 (1956).
34. K. Yosida, Magnetic properties of Cu–Mn alloys. *Phys. Rev.* **106**, 893–898 (1957).
35. J. Kondo, Resistance minimum in dilute magnetic alloys. *Prog. Theor. Exp. Phys.* **32**, 37–49 (1964).
36. C. U. Segre, M. Croft, J. A. Hodges, V. Murgai, L. C. Gupta, B. D. Parks, Valence instability in $\text{Eu}(\text{Pd}_{1-x}\text{Au}_x)_2\text{Si}_2$: The global phase diagram. *Phys. Rev. Lett.* **49**, 1947–1950 (1982).
37. Y. Onuki, M. Hedo, F. Honda, Unique electronic states of Eu-based compounds. *Journal of the Physical Society of Japan* **89**, 102001 (2020).
38. Y. Komijani, P. Coleman, Emergent critical charge fluctuations at the Kondo breakdown of heavy fermions. *Phys. Rev. Lett.* **122**, 217001 (2019).
39. L. Prochaska, X. Li, D. C. MacFarland, A. M. Andrews, M. Bonta, E. F. Bianco, S. Yazdi, W. Schrenk, H. Detz, A. Limbeck, Q. Si, E. Ringe, G. Strasser, J. Kono, S. Paschen, Singular charge fluctuations at a magnetic quantum critical point. *Science* **367**, 285–288 (2020).
40. Z. Ren, L. V. Pourovskii, G. Giriati, G. Lapertot, A. Georges, D. Jaccard, Giant overlap between the magnetic and superconducting phases of CeAu_2Si_2 under pressure. *Phys. Rev. X* **4**, 031055 (2014).
41. K. A. Gschneidner, L. Eyring, Eds., *Handbook on the Physics and Chemistry of Rare Earths, Volume 1: Metals* (North Holland Publishing Company, Amsterdam, 1978).
42. K. A. Gschneidner, L. Eyring, Eds., *Handbook on the Physics and Chemistry of Rare Earths, Volume 2: Alloys and Intermetallics* (North Holland Publishing Company, Amsterdam, 1979).
43. K. T. Moore, G. van der Laan, Nature of the 5f states in actinide metals. *Rev. Mod. Phys.* **81**, 235–298 (2009).
44. S. S. Saxena, P. Agarwal, K. Ahilan, F. M. Grosche, R. K. Haselwimmer, M. Steiner, E. Pugh, I. R. Walker, S. R. Julian, P. Monthoux, G. G. Lonzarich, A. D. Huxley, I. Sheikin, D. Braithwaite, J. Flouquet, Superconductivity on the border of itinerant-electron ferromagnetism in UGe_2 . *Nature* **406**, 587–592 (2000).
45. T. C. Kobayashi, A. Hori, S. Fukushima, H. Hidaka, H. Kotegawa, T. Akazawa, K. Takeda, Y. Ohishi, E. Yamamoto, Pressure-temperature phase diagram and superconductivity in Ulr . *J. Physical Soc. Japan* **76**, 051007 (2007).
46. K. A. Gschneidner, L. Eyring, Eds., *Handbook on the Physics and Chemistry of Rare Earths, Volume 12* (North Holland Publishing Company, Amsterdam, 1989).
47. E. V. Sampathkumaran, R. Vijayaraghavan, Evidence for 4f-ligand dehybridization in the evolution of heavy-fermion behavior in the series $\text{CeCu}_{2-x}\text{Ni}_x\text{Si}_2$. *Phys. Rev. Lett.* **56**, 2861 (1987).
48. S. Süllow, M. C. Aronson, B. D. Rainford, P. Haen, Doniach phase diagram, revisited: From ferromagnet to fermi liquid in pressurized CeRu_2Ge_2 . *Phys. Rev. Lett.* **82**, 2963–2966 (1999).
49. M. B. Fontes, M. A. Continentino, S. L. Bud'ko, M. El-Massalami, L. C. Sampaio, A. P. Guimarães, E. Baggio-Saitovitch, M. F. Hundley, A. Lacerda, Physical properties of the $\text{Ce}(\text{Ru}_{1-x}\text{Fe}_x)_2\text{Ge}_2$ series. *Phys. Rev. B* **53**, 11678–11684 (1996).
50. L. C. Gupta, D. E. MacLaughlin, C. Tien, C. Godart, M. A. Edwards, R. D. Parks, Magnetic behavior of the Kondo-lattice system CeRu_2Si_2 . *Phys. Rev. B* **28**, 3673–3676 (1983).
51. K. Hiebl, C. Horvath, P. Rogl, Magnetic behaviour of ternary silicides CeT_2Si_2 ($T = \text{Ru, Rh, Pd, Os, Ir, Pt}$) and boron substitution in $\text{Ce}(\text{Ru,Os})_2\text{Si}_{2-x}\text{B}_x$. *J. Less Common Met.* **117**, 375–383 (1986).
52. M. Mihalik, V. Sechovsky, Electrical transport and magnetism in CeFe_2Si_2 single crystal. *Physica B* **359–361**, 163–165 (2005).
53. H. Abe, K. Yoshii, H. Kitazawa, Complex magnetic phase diagram of CeRh_2Ge_2 . *Physica B* **312**, 253–255 (2002).
54. R. Movshovich, T. Graf, D. Mandrus, J. D. Thompson, J. L. Smith, Z. Fisk, Superconductivity in heavy-fermion CeRh_2Si_2 . *Phys. Rev. B Condens. Matter* **53**, 8241–8244 (1996).
55. R. Settai, A. Misawa, S. Araki, M. Kosaki, K. Sugiyama, T. Takeuchi, K. Kindo, Y. Haga, E. Yamamoto, Y. Ōnuki, Single crystal growth and magnetic properties of CeRh_2Si_2 . *J. Physical Soc. Japan* **66**, 2260–2263 (1997).
56. M. Mihalik, M. Diviš, V. Sechovský, Electronic and crystal structure of α - and β - CeIr_2Si_2 . *Physica B* **404**, 3191–3194 (2009).
57. H. Fujii, E. Ueda, Y. Uwatoko, T. Shigeoka, Magnetic properties of CeCo_2Ge_2 and NdCo_2Ge_2 single crystals. *J. Magn. Magn. Mater.* **76**, 179–181 (1988).
58. B. Chevalier, J. Etourneau, J. Rossat-Mignod, R. Calemczuk, E. Bonjour, Evolution from the antiferromagnetic to the intermediate valence state in the $\text{Ce}(\text{Rh}_{1-x}\text{Co}_x)_2\text{Si}_2$ system. *J. Phys. Condens. Matter* **3**, 1847–1854 (1991).
59. H. Wilhelm, D. Jaccard, Calorimetric and transport investigations of $\text{CePd}_{2+x}\text{Ge}_{2-x}$ ($x = 0$ and 0.02) up to 22 GPa. *Phys. Rev. B* **66**, 064428 (2002).
60. F. M. Grosche, P. Agarwal, S. R. Julian, N. J. Wilson, R. K. W. Haselwimmer, S. J. S. Lister, N. D. Mathur, F. V. Carter, S. S. Saxena, G. G. Lonzarich, Anomalous low temperature states in CeNi_2Ge_2 and CePd_2Si_2 . *J. Phys. Condens. Matter* **12**, L533–L540 (2000).
61. G. Knebel, M. Brando, J. Hemberger, M. Nicklas, W. Trinkl, A. Loidl, Magnetic, calorimetric, and transport properties of $\text{Ce}(\text{Pd}_{1-x}\text{Ni}_x)_2\text{Ge}_2$ and $\text{CeNi}_2(\text{Ge}_{1-y}\text{Si}_y)_2$. *Phys. Rev. B* **59**, 12390–12397 (1999).
62. A. Thamizhavel, R. Kulkarni, S. K. Dhar, Anisotropic magnetic properties of CeAg_2Ge_2 single crystals. *Phys. Rev. B* **75**, 144426 (2007).
63. C. L. Huang, V. Fritsch, W. Kitzler, H. v. Löhneysen, Low-temperature properties of CeAu_2Ge_2 single crystals grown from Au–Ge and Sn flux. *Phys. Rev. B Condens. Matter* **86**, 214401 (2012).
64. C. S. Garde, J. Ray, Antiferromagnetism in CeAu_2Si_2 - and CeAg_2Si_2 -based Kondo-lattice systems. *J. Phys. Condens. Matter* **6**, 8585–8598 (1994).
65. G. W. Scheerer, Z. Ren, G. Lapertot, G. Garbarino, D. Jaccard, Heavy-fermion superconductivity in CeAg_2Si_2 —Interplay of spin and valence fluctuations. *Physica B Condens. Matter* **536**, 150–154 (2018).
66. O. Trovarelli, M. Weiden, R. Müller-Reisener, M. Gómez-Berisso, P. Gegenwart, M. Deppe, C. Geibel, J. G. Sereni, F. Steglich, Evolution of magnetism and superconductivity in $\text{CeCu}_2(\text{Si}_{1-x}\text{Ge}_x)_2$. *Phys. Rev. B* **56**, 678–685 (1997).
67. D. Jaccard, K. Behnia, J. Sierro, Pressure induced heavy fermion superconductivity of CeCu_2Ge_2 . *Phys. Lett. A* **163**, 475–480 (1992).
68. T. Ooshima, M. Ishikawa, Anomalous magnetic phase diagram of $\text{Ce}(\text{Rh}_{1-x}\text{Co}_x)_2\text{Ge}_2$. *J. Physical Soc. Japan* **67**, 3251–3255 (1998).
69. R. Tripathi, D. Das, C. Geibel, S. K. Dhar, Z. Hossain, Non-fermi-liquid behavior at the antiferromagnetic quantum critical point in the heavy-fermion system $\text{Ce}(\text{Cu}_{1-x}\text{Co}_x)_2\text{Ge}_2$. *Phys. Rev. B* **98**, 165136 (2018).
70. K. Cheng, X. He, H. Yang, B. Zhou, Y. Li, Y. Luo, Synthesis and physical properties of CeRu_2As_2 and CeIr_2As_2 . *Phys. Rev. B* **100**, 205121 (2019).
71. T. Fujiwara, K. Kanto, K. Matsubayashi, Y. Uwatoko, T. Shigeoka, Electrical transport properties of ternary phosphides RRu_2P_2 ($R = \text{La, Ce, Pr}$ and Eu) with ThCr_2Si_2 type crystal structure. *J. Phys. Conf. Ser.* **273**, 012112 (2011).

72. M. Reehuis, W. Jeitschko, Structure and magnetic properties of the phosphides CaCo_2P_2 and LnT_2P_2 with ThCr_2Si_2 structure and LnTP with PbFCI structure (Ln = Lanthanoids, T = Fe, Co, Ni). *J. Phys. Chem. Solid* **51**, 961–968 (1990).
73. C. M. Thompson, "Magneto-Structural Correlations in Rare Earth-Cobalt Nitrides," thesis, The Florida State University (2012), vol. 74–02, 124 pp.
74. M. Reehuis, W. Jeitschko, G. Kotzyba, B. Zimmer, X. Hu, Antiferromagnetic order in the ThCr_2Si_2 type phosphides CaCo_2P_2 and CeCo_2P_2 . *J. Alloys Compd.* **266**, 54–60 (1998).
75. T. Shang, Y. H. Chen, W. B. Jiang, Y. Chen, L. Jiao, J. L. Zhang, Z. F. Weng, X. Lu, H. Q. Yuan, Tunable magnetic orders in $\text{CePd}_2\text{As}_{2-x}\text{P}_x$. *J. Phys. Condens. Matter* **26**, 045601 (2014).
76. Y. Lai, S. E. Bone, S. Minasian, M. G. Ferrier, J. Lezama-Pacheco, V. Mocko, A. S. Ditter, S. A. Kozimor, G. T. Seidler, W. L. Nelson, Y.-C. Chiu, K. Huang, W. Potter, D. Graf, T. E. Albrecht-Schmitt, R. E. Baumbach, Ferromagnetic quantum critical point in CePd_2P_2 with Pd→Ni substitution. *Phys. Rev. B* **97**, 224406 (2018).
77. Y. Luo, J. Bao, C. Shen, J. Han, X. Yang, C. Lv, Y. Li, W. Jiao, B. Si, C. Feng, J. Dai, G. Cao, a. Zhu, Magnetism and crystalline electric field effect in ThCr_2Si_2 -type CeNi_2As_2 . *Physica B Condens. Matter* **86**, 245130 (2012).
78. A. Prasad, H. S. Jeevan, C. Geibel, Z. Hossain, Suppression of quadrupolar order on Si Doping in $\text{YbRu}_2(\text{Ge}_{1-x}\text{Si}_x)_2$. *J. Phys. Condens. Matter* **22**, 126004 (2010).
79. K. Hiebl, C. Horvath, P. Rogl, M. J. Sienko, Magnetic properties and structural chemistry of ternary silicides (RE,Th,U) Ru_2Si_2 (RE = rare earth). *J. Magn. Magn. Mater.* **37**, 287–296 (1983).
80. J. Larrea, M. B. Fontes, E. M. B.-Saitovitch, J. Plessel, M. M. Abd-Elmeguid, J. Ferstl, C. Geibel, A. Pereira, A. Jornada, M. A. Continentino, Phase diagram of the heavy fermion system YbFe_2Ge_2 under pressure. *Phys. Rev. B* **74**, 140406 (2006).
81. J. A. Hodges, Magnetic ordering of ytterbium in YbCo_2Si_2 and YbFe_2Si_2 . *Europhysics Lett.* **4**, 749–753 (1987).
82. M. Francois, G. Venturini, J. F. Maréché, B. Malaman, B. Roques, De Nouvelles Séries de Germaniures, Isotypes de $\text{U}_4\text{Re}_7\text{Si}_6$, ThCr_2Si_2 et CaBe_2Ge_2 , dans les Systèmes Ternaires R T Ge où R est un Elément des Terres Rares et T = Ru, Os, Rh, Ir. *Supraconductivité de L'alr₂Ge₂*. *J. Less Common Met.* **113**, 231–237 (1985).
83. H. Q. Yuan, M. Nicklas, Z. Hossain, C. Geibel, F. Steglich, Quantum phase transition in the heavy-fermion compound YbIr_2Si_2 . *Phys. Rev. B* **74**, 212403 (2006).
84. J. Custers, P. Gegenwart, H. Wilhelm, K. Neumaier, Y. Tokiwa, O. Trovarelli, C. Geibel, F. Steglich, C. Pépin, P. Coleman, The break-up of heavy electrons at a quantum critical point. *Nature* **424**, 524–527 (2003).
85. O. Trovarelli, C. Geibel, M. Grosche, R. Schleser, R. Borth, G. Sparn, F. Steglich, Low-temperature properties of YbCo_2Ge_2 . *Physica B Condens. Matter* **259-261**, 140–141 (1999).
86. M. Kolenda, A. Szytula, The valence state of Yb in YbCo_2Si_2 and YbCo_2Ge_2 compounds on the basis of magnetic susceptibility measurements. *J. Magn. Magn. Mater.* **79**, 57–60 (1989).
87. C. Klingner, C. Krellner, M. Brando, C. Geibel, F. Steglich, Magnetic behaviour of the intermetallic compound YbCo_2Si_2 . *New J. Phys.* **13**, 083024 (2011).
88. Y. D. Seropegin, O. L. Borisenko, O. I. Bodak, V. N. Nikiforov, M. V. Kovachikova, Y. V. Kochetkov, Investigation of phase relationships and physical properties of $\text{Yb}_2\text{Pd}_2\text{Ge}$ compounds. *J. Alloys Compd.* **216**, 259–263 (1995).
89. S. K. Dhar, E. V. Sampathkumaran, R. Vijayaraghavan, R. Kuentzler, YbPd_2Si_2 , A moderate heavy fermion system. *Solid State Commun.* **61**, 479–481 (1987).
90. G. Knebel, D. Braithwaite, G. Lapertot, P. C. Canfield, J. Flouquet, Magnetically ordered Kondo lattice in YbNi_2Ge_2 at high pressure. *J. Phys. Condens. Matter* **13**, 10935–10946 (2001).
91. P. Bonville, J. A. Hodges, P. Imbert, G. Jéhanno, D. Jaccard, J. Sierro, Magnetic ordering and paramagnetic relaxation of Yb^{3+} in YbNi_2Si_2 . *J. Magn. Magn. Mater.* **97**, 178–186 (1991).
92. A. Grytsiv, D. Kaczorowski, V. H. Tran, A. Leithe-Jasper, P. Rogl, Crystal structure and physical properties of Yb-based intermetallics $\text{Yb}(\text{Cu},\text{Ag})_2(\text{Si},\text{Ge})_2$, $\text{Yb}(\text{Cu}_{1-x}\text{Zn}_x)_2\text{Si}_2$ ($x = 0.65, 0.77$) and $\text{Yb}(\text{Ag}_{0.18}\text{Si}_{0.82})_2$. *J. Alloys Compd.* **504**, 1–6 (2010).
93. J. Kaštil, M. Mišek, J. Kamarád, Z. Arnold, K. Vlášková, J. Prchal, M. Diviš, P. Doležal, J. Prokleška, J. Valenta, J. Fikáček, A. Rudajevová, D. Krieger, Properties of the divalent-Yb compound YbAu_2Si_2 under extreme conditions. *Physica B Condens. Matter* **505**, 41–44 (2017).
94. A. Miyake, F. Honda, R. Settai, K. Shimizu, Y. Onuki, Development of the valence fluctuation in the nearly divalent compound YbCu_2Ge_2 under high pressure. *J. Physical Soc. Japan* **81**, S8054 (2012).
95. A. Fernandez-Pañella, V. Balédent, D. Braithwaite, L. Paololini, R. Verbeni, G. Lapertot, J.-P. Rueff, Valence instability of YbCu_2Si_2 through its magnetic quantum critical point. *Physical Review B* **86**, 125104 (2012).
96. T. Nakano, M. Hedo, Y. Uwatoko, E. V. Sampathkumaran, High pressure effects on the electrical resistivity behavior of the Kondo lattice, YbPd_2Si_2 . *Solid State Commun.* **132**, 325–328 (2004).
97. S. Lausberg, A. Hannaske, A. Steppke, L. Steinke, T. Gruner, L. Pedrero, C. Krellner, C. Klingner, M. Brando, C. Geibel, F. Steglich, Doped YbRh_2Si_2 : Not only ferromagnetic correlations but ferromagnetic order. *Phys. Rev. Lett.* **110**, 256402 (2013).
98. J. A. Hodges, G. Jehanno, J. M. Friedt, Hyperfine interactions on ^{151}Eu and ^{57}Fe in amorphous EuFe_2Si_2 . *Hyperfine Interact.* **27**, 365–368 (1986).
99. I. Nowik, I. Felner, Large crystalline fields and anisotropic vibrational modes of $^{151}\text{Eu}^{2+}$ in metallic EuRu_2Ge_2 . *Physica B+C* **130**, 433–435 (1985).
100. A. Prasad, V. K. Anand, Z. Hossain, P. L. Paulose, C. Geibel, Anisotropic magnetic behavior in EuRu_2Ge_2 single crystal. *J. Phys. Condens. Matter* **20**, 285217 (2008).
101. R. E. Gladyshevskii, E. Parthe, Crystal structure of europium dirhodium digermanium, EuRh_2Ge_2 with ThCr_2Si_2 type. *Z. Kristallogr.* **198**, 173–174 (1992).
102. A. Mitsuda, S. Hamano, N. Araoka, H. Yayama, H. Wada, Pressure-induced valence transition in antiferromagnet EuRh_2Si_2 . *J. Physical Soc. Japan* **81**, 023709 (2012).
103. Y. Ashitomi, M. Kakihana, F. Honda, A. Nakamura, D. Aoki, Y. Uwatoko, M. Nakashima, Y. Amako, T. Takeuchi, T. Kida, T. Tahara, M. Hagiwara, Y. Haga, M. Hedo, T. Nakama, Y. Ōnuki, Magnetic properties and effect of pressure on the electronic state of EuCo_2Ge_2 . *Physica B Condens. Matter* **536**, 192–196 (2018).
104. S. Seiro, Y. Prots, K. Kummer, H. Rosner, R. C. Gil, C. Geibel, Charge, lattice and magnetism across the valence crossover in EuRu_2Si_2 single crystals. *J. Phys. Condens. Matter* **31**, 305602 (2019).
105. P. Maślankiewicz, J. Szade, Valence instability of europium in EuCo_2Si_2 . *J. Alloys Compd.* **423**, 69–73 (2006).
106. T. Takeuchi, T. Yara, Y. Ashitomi, W. Iha, M. Kakihana, M. Nakashima, Y. Amako, F. Honda, Y. Homma, D. Aoki, Y. Uwatoko, T. Kida, T. Tahara, M. Hagiwara, Y. Haga, M. Hedo, T. Nakama, Y. Ōnuki, Effects of magnetic field and pressure on the valence-fluctuating antiferromagnetic compound EuPt_2Si_2 . *J. Physical Soc. Japan* **87**, 074709 (2018).
107. E. V. Sampathkumaran, L. C. Gupta, R. Vijayaraghavan, K. V. Gopalakrishnan, R. G. Pillay, H. G. Devare, A new and unique Eu-based mixed valence system: EuPd_2Si_2 . *J. Phys. C Solid State Phys.* **14**, L237–L241 (1981).
108. H. Wada, Y. Goki, A. Mitsuda, Transport properties of EuNi_2Ge_2 under high pressure. *J. Physical Soc. Japan* **87**, 034707 (2018).
109. R. Nagarajan, S. Patil, L. C. Gupta, R. Vijayaraghavan, ^{151}Eu Mössbauer studies in EuNiSi_2 —A new mixed valence system—and in EuNi_2Si_2 and EuNiSi_3 . *J. Magn. Magn. Mater.* **54–57**, 349–350 (1986).
110. I. Schellenberg, W. Hermes, S. Lidin, R. Pottgen, Structure and properties of the 5.5 K antiferromagnet EuAu_2Ge_2 . *Z. Kristallogr.* **226**, 214–218 (2011).
111. H.-J. Hesse, G. Wortmann, ^{151}Eu -Mössbauer study of pressure induced valence transitions in EuM_2Ge_2 ($M = \text{Ni}, \text{Pd}, \text{Pt}$). *Hyperfine Interact.* **91**, 1499–1504 (1994).
112. E. R. Bauminger, I. Felner, D. Froindlich, D. Levron, I. Nowik, S. Ofer, R. Yanovsky, Mössbauer effect studies of interconfiguration fluctuations in metallic rare earth compounds. *J. Phys. Colloq.* **35**, C6–C70 (1974).
113. G. Bulk, W. Nolting, Antiferromagnetism in 4f-systems with valence instabilities. *Z. Physik B Condens. Matter* **70**, 473–483 (1988).
114. J. Gouchi, K. Miyake, W. Iha, M. Hedo, T. Nakama, Y. Onuki, Y. Uwatoko, Quantum criticality of valence transition for the unique electronic state of antiferromagnetic compound EuCu_2Ge_2 . *J. Physical Soc. Japan* **89**, 053703 (2020).
115. B. C. Sales, R. Viswanathan, Demagnetization due to interconfiguration fluctuations in the RE-Cu₂Si₂ compounds. *J. Low Temp. Phys.* **23**, 449–467 (1976).
116. P. G. Pagliuso, J. L. Sarrao, J. D. Thompson, M. F. Hundley, M. S. Sercheli, R. R. Urbano, C. Rettori, Z. Fisk, S. B. Oseroff, Antiferromagnetic ordering of divalent Eu in EuCu_2Si_2 single crystals. *Phys. Rev. B* **63**, 092406 (2001).
117. W. H. Jiao, I. Felner, I. Nowik, G. H. Cao, EuRu_2As_2 : A new ferromagnetic metal with collapsed ThCr_2Si_2 -type structure. *J. Supercond. Nov. Magn.* **25**, 441–445 (2012).
118. T. Terashima, M. Kimata, H. Satsukawa, A. Harada, K. Hazama, S. Uji, H. S. Suzuki, T. Matsumoto, K. Murata, EuFe_2As_2 under high pressure: An antiferromagnetic bulk superconductor. *J. Physical Soc. Japan* **78**, 083701 (2009).
119. P. Proschek, J. Prchal, M. Diviš, J. Prokleška, K. Vlášková, J. Valenta, J. Zubáč, J. Kaštil, M. Hedo, T. Nakama, Y. Ōnuki, F. Honda, Weakly anisotropic ferromagnet EuRu_2P_2 : Ambient and hydrostatic pressure characterization. *J. Alloys Compd.* **864**, 158753 (2021).
120. C. Feng, Z. Ren, S. Xu, S. Jiang, Z. Xu, G. Cao, I. Nowik, I. Felner, K. Matsubayashi, Y. Uwatoko, Magnetic ordering and dense Kondo behavior in EuFe_2P_2 . *Phys. Rev. B* **82**, 094426 (2010).
121. Y. Singh, Y. Lee, B. N. Harmon, D. C. Johnston, Unusual magnetic, thermal, and transport behavior of single-crystalline EuRh_2As_2 . *Phys. Rev. B* **79**, 220401 (2009).
122. M. Bishop, W. Uehoy, G. Tsoi, Y. K. Vohra, A. S. Sefat, B. C. Sales, Formation of collapsed tetragonal phase in EuCo_2As_2 under high pressure. *J. Phys. Condens. Matter* **22**, 425701 (2010).
123. M. Reehuis, W. Jeitschko, M. H. Möller, P. J. Brown, A neutron diffraction study of the magnetic structure of EuCo_2P_2 . *J. Phys. Chem. Solid* **53**, 687–690 (1992).
124. D. Nakamura, M. Hedo, K. Uchima, Y. Takaesu, T. Nakama, K. Yagasaki, T. Fujiwara, T. Shigeoka, T. Matsumoto, Y. Uwatoko, Effects of pressure and magnetic field on transport properties of EuCo_2P_2 . *J. Physical Soc. Japan* **3**, 011036 (2014).

125. G. Michels, M. Roepke, T. Niemöller, M. Chefki, M. M. Abd-Elmeguid, H. Micklitz, E. Holland-Moritz, W. Schlabit, C. Huhnt, B. Buchner, A. Wurth, A. Mewis, V. Kataev, The anomalous valence state of Eu and magnetic order in EuRh_2P_2 . *J. Phys. Condens. Matter* **8**, 4055–4062 (1996).
126. W. L. Nelson, A. S. Jayasinghe, D. Graf, S. Lattner, R. E. Baumbach, Electronic and magnetic properties of $\text{EuNi}_{2-x}\text{Sb}_2$ structural variants. *J. Phys. Condens. Matter* **32**, 315801 (2020).
127. V. K. Anand, D. C. Johnston, Physical properties of EuPd_2As_2 single crystals. *J. Phys. Condens. Matter* **26**, 286002 (2014).
128. G. Drachuk, A. E. Bohmer, S. L. Bud'ko, P. C. Canfield, Magnetization and transport properties of single crystalline RPd_2P_2 (R=Y, La-Nd, Sm-Ho, Yb). *J. Magn. Magn. Mater.* **417**, 420–433 (2016).
129. W. T. Jin, N. Qureshi, Z. Bukowski, Y. Xiao, S. Nandi, M. Babji, Z. Fu, Y. Su, T. Brückel, Spiral magnetic ordering of the Eu moments in EuNi_2As_2 . *Phys. Rev. B* **99**, 014425 (2019).
130. Y. Hirayama, A. Nakamura, M. Hedo, T. Takeuchi, A. Mori, Y. Hirose, K. Mitamura, K. Sugiyama, M. Hagiwara, T. Nakama, Y. Ōnuki, Heavy fermion state based on the Kondo effect in EuNi_2P_2 . *J. Physical Soc. Japan* **82**, 083708 (2013).
131. S. Danzenbächer, D. V. Vyalikh, Y. Kucherenko, A. Kade, C. Laubschat, N. Caroca-Canales, C. Krellner, C. Geibel, A. V. Fedorov, D. S. Dessau, R. Follath, W. Eberhardt, S. L. Molodtsov, Hybridization phenomena in nearly-half-filled f-shell electron systems: Photoemission study of EuNi_2P_2 . *Phys. Rev. Lett.* **102**, 026403 (2009).
132. K. Hiebl, C. Horvath, P. Rogl, M. J. Sienko, Magnetic properties and structural data of ternary silicides: $(\text{RE,Th,U})\text{Os}_2\text{Si}_2$ (RE = rare earth). *Solid State Commun.* **48**, 211–215 (1983).
133. H. M. Duh, I. S. Lyubutin, I. M. Jiang, G. H. Hwang, K. D. Lain, Magnetic properties of $\text{U}(\text{Pd}_{1-x}\text{Fe}_x)_2\text{Ge}_2$. *J. Magn. Magn. Mater.* **153**, 86–96 (1996).
134. A. Szytuła, Ł. Gondek, M. Ślaski, B. Penc, A. Jezierski, Non-magnetic behaviour of UFe_2Si_2 compound. *J. Alloys Compd.* **442**, 275–278 (2007).
135. S. Süllow, G. J. Nieuwenhuys, A. A. Menovsky, J. A. Mydosh, S. A. M. Mentink, T. E. Mason, W. J. L. Buyers, Spin glass behavior in URh_2Ge_2 . *Phys. Rev. Lett.* **78**, 354–357 (1997).
136. H. Ptasiwicz-Bak, Neutron diffraction study of magnetic ordering in UPd_2Si_2 , UPd_2Ge_2 , URh_2Si_2 and URh_2Ge_2 . *J. Phys. F Met. Phys.* **11**, 1225–1235 (1981).
137. M. Kuznietz, H. Pinto, H. Etedgui, M. Melamud, Neutron-diffraction study of the magnetic structure of UCo_2Ge_2 . *Phys. Rev. B* **40**, 7328–7331 (1989).
138. T. Endstra, G. J. Nieuwenhuys, A. A. Menovsky, J. A. Mydosh, Structural and magnetic properties of UCo_2Ge_2 . *J. Appl. Phys.* **69**, 4816–4818 (1991).
139. L. Chelmicki, J. Leciejewicz, A. Zygmunt, Magnetic properties of UT_2Si_2 and UT_2Ge_2 (T = Co, Ni, Cu) intermetallic systems. *J. Phys. Chem. Solid* **46**, 529–538 (1985).
140. M. Mihalik, A. Kolomiets, J.-C. Griveau, A. V. Andreev, V. Sechovsky, Magnetism of UCo_2Si_2 single crystal studied under applied magnetic field and hydrostatic pressure. *High Press. Res.* **26**, 479–483 (2007).
141. G. Quirion, F. S. Razavi, M. L. Plumer, J. D. Garrett, Pressure-temperature phase diagram of UPd_2Si_2 and UNi_2Si_2 . *Phys. Rev. B* **57**, 5220–5224 (1998).
142. S. B. Roy, A. K. Pradhan, P. Chaddah, Magnetic properties of polycrystalline UNi_2Ge_2 : Irreversibility and metastable behaviour. *J. Phys. Condens. Matter* **6**, 5155–5160 (1994).
143. C. Tabata, N. Miura, K. Uhlřřova, M. Vališka, H. Saito, H. Hidaka, T. Yanagisawa, V. Sechovský, H. Amitsuka, Peculiar magnetism of UAu_2Si_2 . *Phys. Rev. B* **94**, 214414 (2016).
144. T. D. Matsuda, S. Ikeda, E. Yamamoto, Y. Haga, Y. Onuki, Magnetic property of a single crystal UCu_2Ge_2 . *J. Physical Soc. Japan* **76**, 074708 (2007).
145. T. D. Matsuda, Y. Haga, S. Ikeda, A. Galatanu, E. Yamamoto, H. Shishido, M. Yamada, J.-I. Yamaura, M. Hedo, Y. Uwatoko, T. Matsumoto, T. Tada, S. Noguchi, T. Sugimoto, K. Kuwahara, K. Iwasa, M. Kohgi, R. Settai, Y. Ōnuki, Electrical and magnetic properties of a single crystal UCu_2Si_2 . *J. Physical Soc. Japan* **74**, 1552–1556 (2005).
146. Z. Fisk, N. O. Moreno, J. D. Thompson, Properties of Cu-flux-grown UCu_2Si_2 . *J. Phys. Condens. Matter* **15**, S1917–S1921 (2003).
147. M. A. Avila, S. L. Bud'ko, P. C. Canfield, Anisotropic magnetization, specific heat and resistivity of RFe_2Ge_2 single crystals. *J. Magn. Magn. Mater.* **270**, 51–76 (2004).
148. I. Felner, J. Nowik, Magnetism and hyperfine interactions in EuM_2Ge_2 and GdM_2Ge_2 (M = Mn, Fe, Co, Ni, Cu). *J. Phys. Chem. Solid* **39**, 767–773 (1978).
149. A. Gallagher, K. W. Chen, C. M. Moir, S. K. Cary, F. Kametani, N. Kikugawa, D. Graf, T. E. Albrecht-Schmitt, S. C. Riggs, A. Shekhter, R. E. Baumbach, Unfolding the physics of URu_2Si_2 through silicon to phosphorus substitution. *Nat. Commun.* **7**, 10712 (2016).
150. Y. Dalichaouch, M. B. Maple, J. W. Chen, T. Kohara, C. Rossel, M. S. Torikachvili, A. L. Giorgi, Effect of transition-metal substitutions on competing electronic transitions in the heavy-electron compound URu_2Si_2 . *Physica B Condens. Matter* **41**, 1829–1836 (1990).

Acknowledgments

Funding: R.E.B. acknowledges support from the National Science Foundation through NSF DMR-1904361. Y.L. was supported in part by the Center for Actinide Science and Technology, an Energy Frontier Research Center funded by the U.S. Department of Energy (DOE), Office of Science, Basic Energy Sciences (BES), under Award Number DE-SC0016568. J.Y.C. acknowledges NSF DMR-2209804 and Welch Grant number AT-2056-20210327 for partial support. The National High Magnetic Field Laboratory is supported by the National Science Foundation through NSF DMR-1644779 and the State of Florida. We acknowledge J. Ortega for drawing the crystal structures. We thank C. McNiel (NHMFL) for essential contributions in designing Figs. 3 to 6. **Author contributions:** R.E.B. conceived the project. All authors contributed equally to the compilation of data from the literature, its interpretation, and writing. J.Y.C. is primarily responsible for studies of composite structures that are referenced. **Competing interests:** The authors declare that they have no competing interests. **Data and materials availability:** All data needed to evaluate the conclusions in the paper are present in the paper and are available in the references.

Submitted 1 March 2022

Accepted 27 June 2022

Published 10 August 2022

10.1126/sciadv.abp8264

Electronic landscape of the *f*-electron intermetallics with the ThCr₂Si₂ structure

You Lai, Julia Y. Chan, and Ryan E. Baumbach

Sci. Adv. **8** (31), eabp8264. DOI: 10.1126/sciadv.abp8264

View the article online

<https://www.science.org/doi/10.1126/sciadv.abp8264>

Permissions

<https://www.science.org/help/reprints-and-permissions>

Use of this article is subject to the [Terms of service](#)

Science Advances (ISSN 2375-2548) is published by the American Association for the Advancement of Science, 1200 New York Avenue NW, Washington, DC 20005. The title *Science Advances* is a registered trademark of AAAS.

Copyright © 2022 The Authors, some rights reserved; exclusive licensee American Association for the Advancement of Science. No claim to original U.S. Government Works. Distributed under a Creative Commons Attribution NonCommercial License 4.0 (CC BY-NC).